OPEN

Rational Design of Pathogen-Mimicking Amphiphilic Materials as Nanoadjuvants

Bret D. Ulery[1]*, Latrisha K. Petersen[1]*, Yashdeep Phanse[2], Chang Sun Kong[3], Scott R. Broderick[3], Devender Kumar[4], Amanda E. Ramer-Tait[2], Brenda Carrillo-Conde[1], Krishna Rajan[3], Michael J. Wannemuehler[2], Bryan H. Bellaire[2], Dennis W. Metzger[4] & Balaji Narasimhan[1]

[1]Department of Chemical and Biological Engineering, Iowa State University, Ames, IA 50011, [2]Department of Veterinary Microbiology and Preventive Medicine, Iowa State University, Ames, IA 50011, [3]Department of Materials Science and Engineering, Iowa State University, Ames, IA 50011, [4]Center for Immunology and Microbial Disease, Albany Medical College, Albany, NY 12208.

An opportunity exists today for cross-cutting research utilizing advances in materials science, immunology, microbial pathogenesis, and computational analysis to effectively design the next generation of adjuvants and vaccines. This study integrates these advances into a bottom-up approach for the molecular design of nanoadjuvants capable of mimicking the immune response induced by a natural infection but without the toxic side effects. Biodegradable amphiphilic polyanhydrides possess the unique ability to mimic pathogens and pathogen associated molecular patterns with respect to persisting within and activating immune cells, respectively. The molecular properties responsible for the pathogen-mimicking abilities of these materials have been identified. The value of using polyanhydride nanovaccines was demonstrated by the induction of long-lived protection against a lethal challenge of *Yersinia pestis* following a single administration ten months earlier. This approach has the tantalizing potential to catalyze the development of next generation vaccines against diseases caused by emerging and re-emerging pathogens.

O ver the centuries, control of infectious diseases has often been hampered by the use of suboptimal tools and a lack of knowledge to prevent the spread of epidemic and pandemic diseases, including a dearth of efficacious vaccines. A transdisciplinary approach based on a new paradigm of immune activation is needed to rationally design next generation adjuvants and vaccines. Typically, adjuvants fulfill three roles: 1) act as a depot; 2) direct antigen to antigen presenting cells (APCs); and 3) induce co-stimulatory signals on APCs necessary for activation of naïve T cells. Unfortunately, current adjuvants approved for human use are often based on off-the-shelf materials that were not originally intended for use as adjuvants and allow pathogens to evade host defenses. The next generation of efficacious vaccines must incorporate adjuvants that can be tailored to generate the optimal immune response that provides protection against the target pathogen. In this work, we describe a bottom-up approach to design "pathogen-mimicking" nanoparticle adjuvants that has provided new insights into the rational design of customized vaccine delivery vehicles to induce long-lived, protective immunity.

An ideal vaccine will mimic the way in which a naturally occurring infection induces a robust immune response yet avoid the undesirable effects of disease[1]. Current approaches to enhance the efficacy of a vaccine with an adjuvant often are designed to signal the innate immune system through a limited set of germ-line encoded pattern-recognition receptors (PRRs). These receptors recognize a series of conserved pathogen-associated molecular patterns (PAMPs)[2]. The design of non-toxic polymeric materials that activate APCs without deleterious side effects will lead to efficacious vaccine delivery systems while improving patient compliance by reducing the need for prime-boost immunization regimen.

In this regard, degradable polymers are promising candidates for adjuvants and directed delivery vehicles because their properties can be tailored to enhance the immune response[3–5]. While a number of degradable polymer families (polyesters[4], polyethers[6], and polyphosphazenes[7]) have been investigated as vaccine adjuvants, amphiphilic polyanhydrides offer a unique set of properties that allow them to function similarly to traditional adjuvants but without the challenges associated with them (i.e., protein instability, low pH environments, poor control over release kinetics, multiple dose immunization regimens, inclusion of surfactants, stabilizers, etc.)[8]. We

have previously demonstrated that amphiphilic polyanhydride particles release stable proteins in a controlled manner[9,10] while activating APCs and inducing long-lived protective immunity in the absence of additional excipients[5,11–13].

Many chemistry-dependent interactions associated with materials design have been evaluated, including protein stabilization, protein release, and immune activation[3,9–11,13], yet little work to date has investigated the specific material properties responsible for these attributes. The identification of these properties can lead to the rational design of new and safe adjuvants that induce strong immune responses reminiscent of natural infections. Fig. 1 depicts our hypothesis that amphiphilic polyanhydride nanoparticles behave in a manner that mimics the ability of pathogens to induce a robust immune response. To test this hypothesis, we devised a transdisciplinary approach that combines polymer chemistry, cell biology, immunology, and informatics analysis to identify the properties of polyanhydrides that mimic microbial PAMPs. This approach presents a *direct* comparison between polyanhydride nanoparticles and pathogens (i.e., *Escherichia coli* and *Yersinia pestis*) based on their persistence within and ability to activate APCs. We analyzed the ability of the nanoparticles to activate APCs in comparison to lipopolysaccharide (LPS), a PAMP found on the outer membrane of Gram-negative bacteria[14]. Using informatics analysis to evaluate the interactions of APCs with polyanhydride nanoparticles (Fig. 1 left) or pathogens (Fig. 1 right), we have identified molecular attributes that confer "pathogen-like" behavior to amphiphilic polyanhydrides. These insights were used to design and test a single dose nanoparticle vaccine for pneumonic plague that induced long-lived protection against a lethal challenge.

Results

In order to investigate internalization and persistence of nanoparticles within APC, bone marrow-derived dendritic cells (DCs) were incubated with fluorescently labeled polystyrene (PS) beads, 50:50 CPH:SA or 50:50 CPTEG:CPH polyanhydride nanoparticles, *E. coli* or *Y. pestis*. The phagocytic capacity of DCs was assessed using 200 nm and 2 μm PS beads as an inert control. Morphometric analysis was utilized to assess particle/bacteria count as a function of size to determine if the particles/bacteria changed in size (i.e., due to aggregation or degradation) internalization. These morphometric patterns are observed during bacterial internalization, replication and intracellular persistence and can therefore be utilized as a comparison parameter to assess the pathogen mimicking characteristics of nanoparticles. After 2 h, morphometric analysis revealed that the different particle chemistries and the bacteria were similarly internalized by DCs with respect to particle size and the number of particles (Fig. 2a and 2b). Microscopic observations at both 2 and 48 h (Fig. 3a) indicated that the majority of particles were located within late endosomes. These results are consistent with phagosome–lysosome fusion events that are part of the exogenous pathway of antigen uptake, processing, and presentation[16].

The intracellular fate of pathogens (i.e., persistence, replication, rapid degradation) influences the functional capacity of APCs. In order to model the differential responses of the DCs induced by the various treatments, we characterized the intracellular fate of PS beads and polyanhydride nanoparticles, particularly in comparison to that of bacteria. At 48 h, DCs incubated with PS beads contained large numbers of individual (i.e., non-aggregating) particles (Fig. 3a). In contrast, both 50:50 CPH:SA and 50:50 CPTEG:CPH nanoparticles were found to be aggregated within lysosomes. More 50:50 CPTEG:CPH nanoparticles persisted within this intracellular compartment at 48 h (as evidenced by similar size versus number relationships) as compared to 50:50 CPH:SA nanoparticles (Fig. 3b). Because both polyanhydride nanoparticle formulations degraded, our hypothesis is that the amphiphilic 50:50 CPTEG:CPH nanoparticles maintained their size because their degradation was balanced
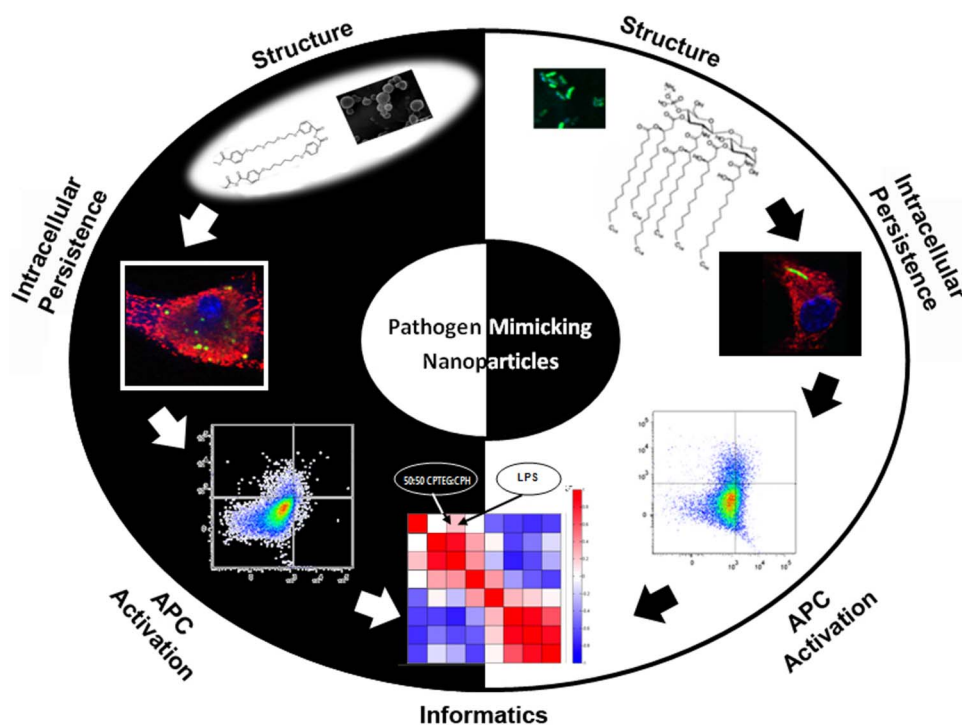

Figure 1 | Cartoon representation of the hypothesis that polyanhydride nanoparticles mimic the immune activation capacity of pathogens. Molecular structures dictate how materials are internalized and processed by APCs, which in turn leads to cellular activation. Utilizing informatics analysis, large data sets can be mined to determine which nanoparticle chemistries (*left*) are able to best mimic pathogen-induced activation of APCs (*right*). Further analysis with this approach allows for the identification of molecular descriptors that are specifically responsible for APC activation. Structures of 50:50 CPTEG:CPH (top left quadrant) and LPS (top right quadrant) were obtained as permitted[15].
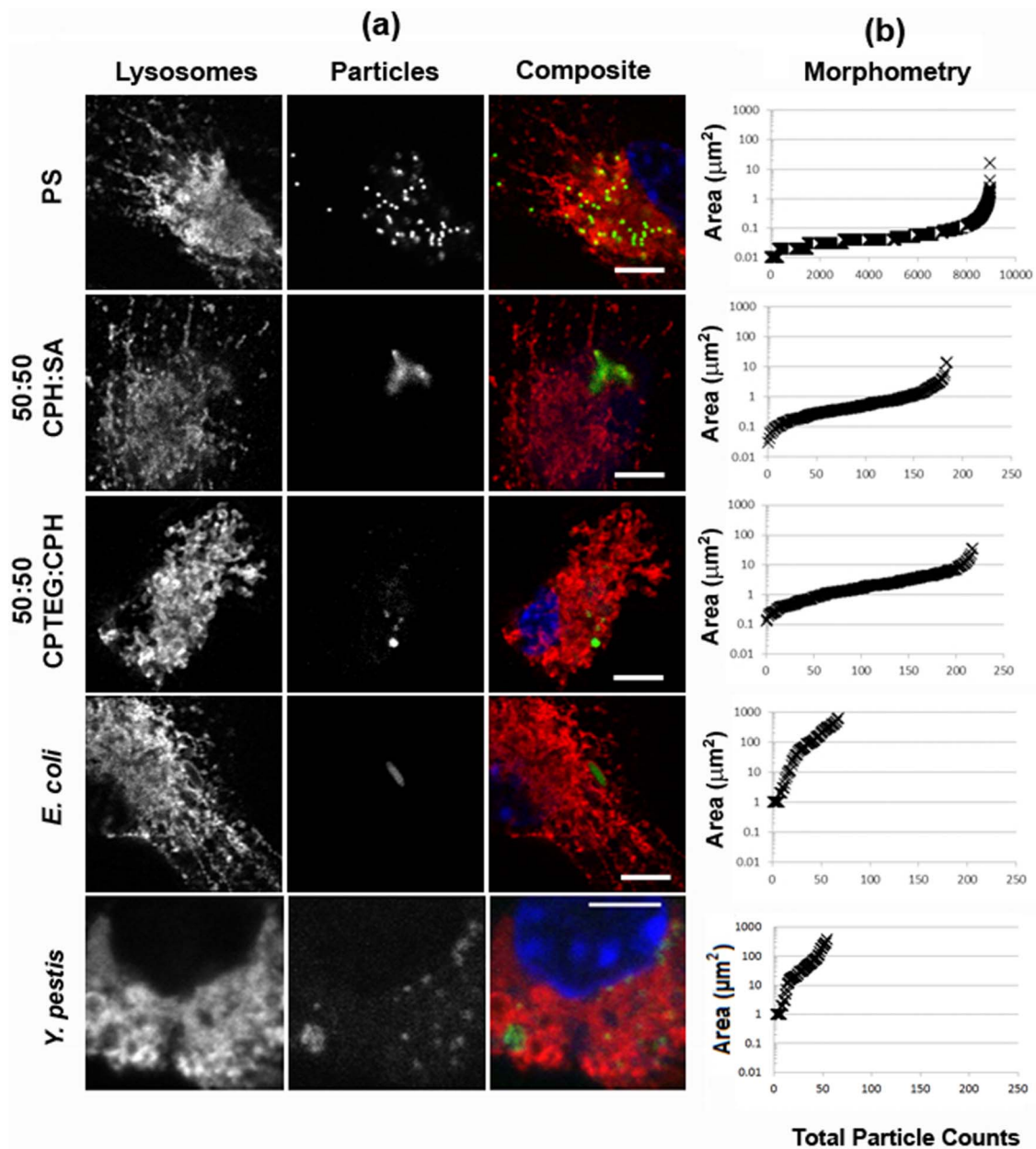
Figure 2 | Internalization of nanoparticles and bacteria (*E. coli* or *Y. pestis*) in dendritic cells at 2 h post-incubation. (a) Mouse DCs were incubated separately with either fluorescently-labeled (green) PS beads (200 nm and 2.0 μm), 50:50 CPH:SA nanoparticles, 50:50 CPTEG:CPH nanoparticles, *E. coli*, or *Y. pestis*. Fluorescent detection of phalloidin⁺ polymerized actin is shown in red. Photomicrographs shown are representative of results obtained from five independent experiments (scale bars = 5 μm). (b) Results were compiled from a morphometric analysis performed on replicate, epifluorescent photomicrographs for each treatment group. For the morphometric analysis at 2 h, data points were ordered based on size (μm²) from smallest to largest along the vertical axis and the total number of particles measured is reflected on the horizontal axis.

by their aggregation, whereas the intracellular aggregation of the hydrophobic 50:50 CPH:SA nanoparticles far exceeds their degradation (Fig. 3b).

When phagocytic cells like DCs internalize pathogens, they create intracellular particulate agglomerates after 48 h as observed in Fig. 3. When compared to *E. coli* and *Y. pestis* internalization (Figs. 2 and 3), the amphiphilic 50:50 CPTEG:CPH nanoparticles appeared to be similarly internalized and persisted at 2 and 48 h, respectively. This persistence of the 50:50 CPTEG:CPH nanoparticles suggests that the stimuli provided by these particles to activate DCs would not rapidly wane, much like that provided by persisting and replicating bacteria[17]. Indeed, comparing morphometric results between intracellular bacteria and internalized 50:50 CPTEG:CPH nanoparticles (Fig. 3b) revealed similar persistence patterns. In contrast,

hydrophobic 50:50 CPH:SA nanoparticles aggregated over time, resulting in larger but fewer particles.

Furthermore, lysosomal localization of the 50:50 CPTEG:CPH nanoparticles provides an optimal location for antigen presentation with concomitant cell activation[18,19]. It is of note that while the majority of the nanoparticles were found within Lamp1⁺ lysosomes at 48 h, a minor portion of intracellular particles were not, and could be either within Lamp1⁻ vesicles or, more likely, free within the cytosol. The capacity for antigen release within both lysosomal and cytosolic compartments could enable cross presentation and enhanced antigen presentation – experiments to test this hypothesis are currently underway in our laboratories.

Given the central role of DCs in the development of robust immune responses, we next assessed the capacity of the polyanhydride
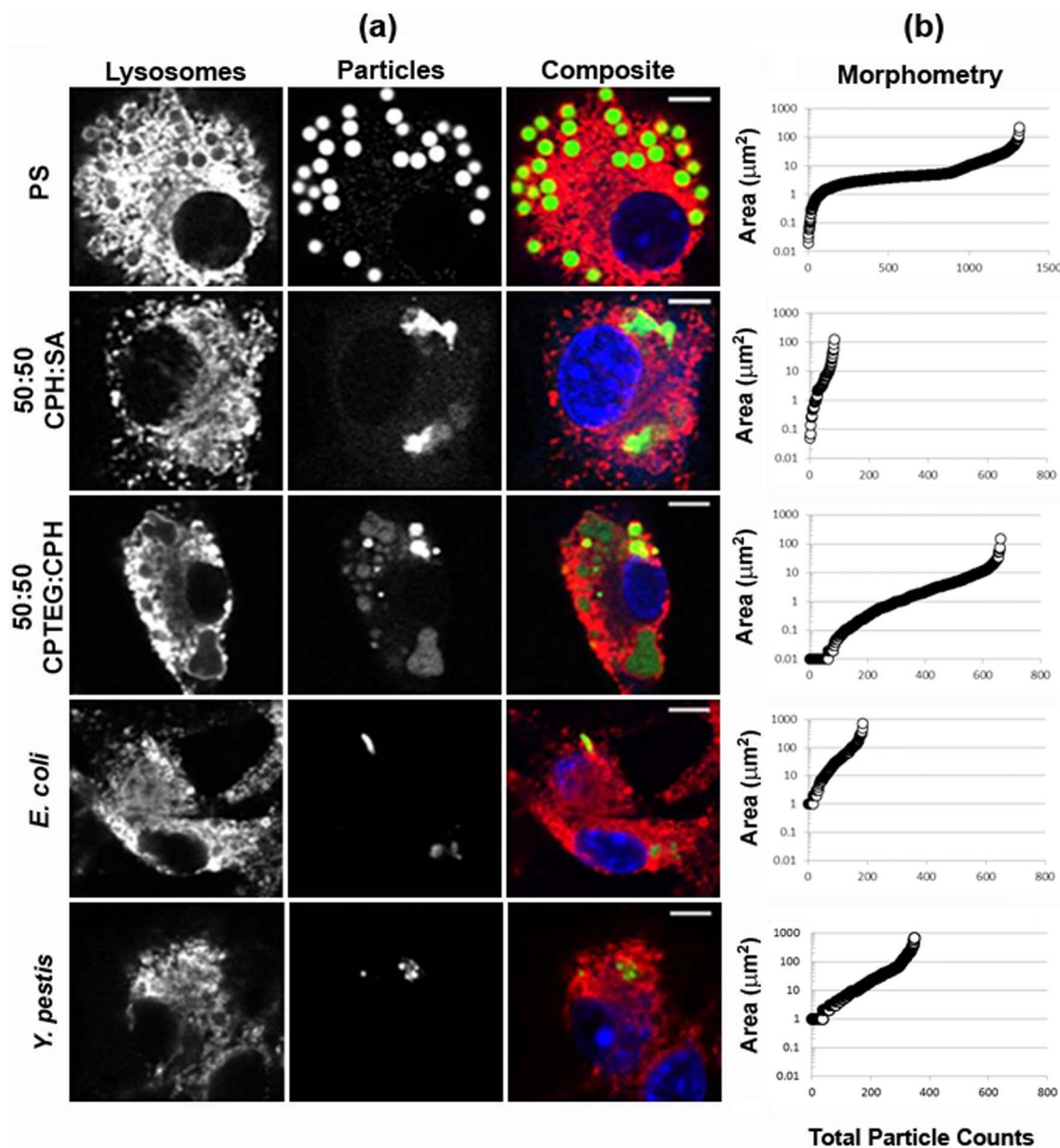
Figure 3 | Persistence of amphiphilic 50:50 CPTEG:CPH nanoparticles and bacteria (*E. coli* or *Y. pestis*) in dendritic cells at 48 h post-incubation. (a) Fluorescent antibody detection of LAMP-1^{+} lysosomes is shown in red. Photomicrographs shown are representative of results obtained from five independent experiments (scale bars = 5 μm). (b) See caption for Figure 2b.

nanoparticles to activate DCs in comparison to LPS. DCs stimulated with hydrophobic 50:50 CPH:SA nanoparticles failed to increase surface expression of major histocompatibility complexes (MHC) I and II and the T cell co-stimulatory molecules CD86 and CD40 over non-stimulated DCs (Fig. 4a). In contrast, stimulation of DCs with amphiphilic 50:50 CPTEG:CPH nanoparticles resulted in a significant increase in all these activation markers over the non-stimulated controls (Fig. 4a). Moreover, 50:50 CPTEG:CPH nanoparticles activated DCs to a similar degree as did treatment with LPS in terms of MHC I, MHC II, and CD86 expression but not CD40 expression (Fig. 4a). Significantly greater quantities of the pro-inflammatory cytokines IL-6, IL-12p40, and TNF-α were secreted from DCs exposed to 50:50 CPH:SA or 50:50 CPTEG:CPH nanoparticles as compared to non-stimulated DCs; however, the amounts of cytokines induced by nanoparticles were far less than those induced by LPS (Fig. 4b). This data reveals a potential benefit of 50:50 CPTEG:CPH nanoparticles as a vaccine adjuvant, because excessive CD40 signaling and pro-inflammatory cytokine production can lead

to adverse consequences. Indeed, mice deficient in CD40 are more resistant to the effects of polymicrobial sepsis, produce less IL-6 and IL-12, and sustain less systemic organ damage than wild-type controls[20]. Together, our data demonstrate that amphiphilic 50:50 CPTEG:CPH nanoparticles possess pathogen-like characteristics that promote DC activation in a tempered context that would likely limit the development of an overwhelming inflammatory response, thus making them excellent vaccine delivery vehicles.

We then investigated the relationships between various polyanhydride chemistries (represented by CPH:SA and CPTEG:CPH copolymers), *E. coli, Y. pestis,* and LPS for intracellular persistence and DC activation using a "blinded" approach to informatics analysis (Fig. 5). Specifically, the trends in these relationships were quantitatively modeled based on a set of molecular descriptors chosen to interrogate pathogen-like behavior. The library of descriptors was built partially on the structural descriptors[21] of CPH:SA and CPTEG:CPH copolymers and microbial components (i.e., LPS) and on experimentally measured descriptors such as glass transition temperature,
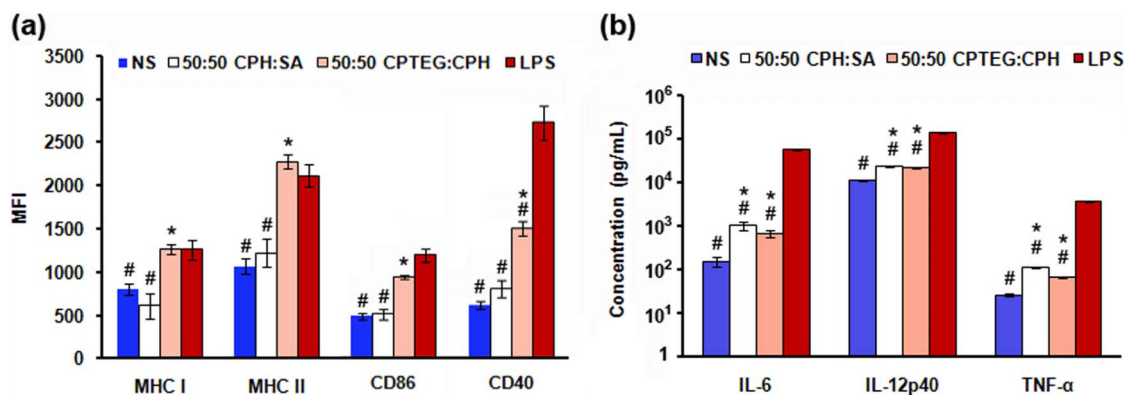
Figure 4 | Polyanhydride nanoparticles generate an activated DC phenotype similar to that of DCs stimulated with LPS. Cell surface marker expression (a) and cytokine secretion (b) for non-stimulated (NS, negative control) DCs, DCs stimulated with LPS (positive control) or nanoparticles composed of either 50:50 CPH:SA or 50:50 CPTEG:CPH for 48 h. A minimum of eight replicates was used per group. Error bars represent standard error. MFI = mean fluorescence intensity. * indicates $p \leq 0.002$ compared to NS and # indicates $p \leq 0.002$ compared to LPS.
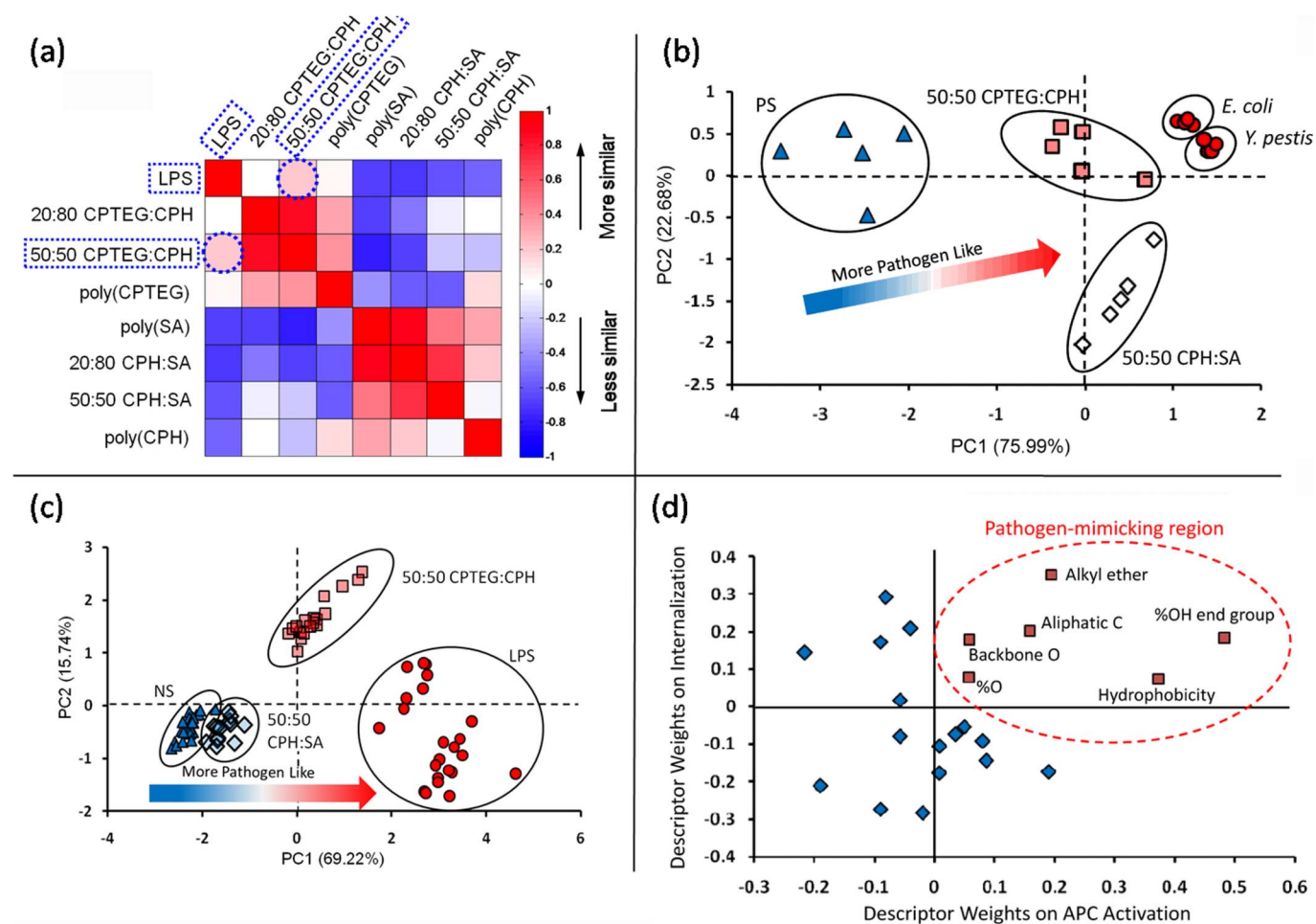

Figure 5 | Informatics analysis using specific molecular descriptors to identify polymer chemistries that behave in a pathogen-like manner.
(a) Similarity (correlation) matrix for the paired comparison of LPS and various polyanhydride copolymers in terms of molecular descriptors; the red color indicates highest similarity and blue represents lowest similarity with LPS. Based on Pearson's correlation, 50:50 CPTEG:CPH showed the highest similarity with LPS (indicated by the blue dotted circles). (b) In terms of intracellular persistence, 50:50 CPTEG:CPH nanoparticles are more pathogen-like than 50:50 CPH:SA or PS. (c) In terms of DC activation, 50:50 CPTEG:CPH nanoparticles are more pathogen-like than 50:50 CPH:SA or NS.
(d) Using a PLS model linking molecular descriptors with the positions of the nanoparticle formulations in panel (b) representing the y-axis and panel (c) representing the x-axis, the descriptors that influence pathogen-like behavior in terms of both nanoparticle persistence and DC activation were identified (relevant descriptors labeled on figure).

Table 1 | Molecular descriptors (1–23) defined by Bicerano[21] and material property measurements (24–28) for the enumeration of polymer and LPS features

ID	Molecular descriptor	Description
1	$^0\chi$	Atomic index 1
2	$^0\chi^v$	Atomic index 2
3	$^1\chi$	Connectivity index 1
4	$^1\chi^v$	Connectivity index 2
5	BB_index1	Backbone index 1
6	BB_index2	Backbone index 2
7	SG_index	Backbone index 3
8	N_SP	Number of atoms in the shortest path across the backbone of a polymeric repeat unit
9	N_C	Number of carbon atoms
10	N_O	Number of oxygen atoms
11	N_H	Number of hydrogen atoms
12	N_ester	Number of backbone -COO-
13	N_ether	Number of -O- in a polymeric repeat unit
14	N_aromatic_ring	Number of aromatic rings in a polymeric repeat unit
15	N_CH_2	Number of CH_2 groups in a polymeric repeat unit
16	N_alkyl_ether	Number of ether (R-O-R′) linkages between two units R and R′ both of which are connected to the alkyl carbon atom
17	N_nh	Total number of non-hydrogen atoms in a repeat unit
18	N_{mv}	2*N_ester+3*N_ether
19	N_K	$-3*(N\_ether)^{-3}*N\_acrylic\_ester$
20	N_rot	Total number of rotational degrees of freedom parameter
21	N_dc	7*N_backbone_O+12*N_side Group_O
22	N_group	-N_alkyl_ether+7*N_CO+2*N_other C=O
23	MW	Molecular weight
24	% OH end group	Percentage of -OH groups
25	Hydrophobicity	Water contact angle
26	% MW loss	Percent loss of polymer molecular weight from NMR and GPC
27	% Erosion	Percent of polymer eroded, from erosion kinetics experiments
28	T_g	Glass transition temperature from DSC

hydrophobicity, and erosion kinetics (Table 1 and Supplementary Data Table 1). Thermal properties of LPS are known and correlate closely with those of whole bacteria[22,23]. The chemical and structural similarities between the polyanhydride chemistries and LPS were explored using a correlation similarity metric[24], where similarity was defined by the proximity between chemistries in the descriptor space. Of the polymer formulations evaluated, the similarity plot shown in Fig. 5a demonstrates that the amphiphilic 50:50 CPTEG:CPH has the highest similarity with LPS.

Using principal component analysis (PCA), we identified the relationships between various polyanhydride formulations and pathogens or LPS in the context of intracellular persistence and DC activation (Fig. 5b and 5c, respectively)[25]. An Euclidean geometrical mapping metric that considers both the distance between two points as well as the angle between point-origin-point was used to identify similarity in the attributes associated with the targeted functionality of pathogen-like behavior. For both intracellular persistence (Fig. 5b) and DC activation (Fig. 5c) data, the angular direction of correlation was drawn as an arrow and defined based on maximizing the difference between the target (i.e., LPS or bacteria) and the nanoparticle formulations. The geometrical proximity of the angular projection of the 50:50 CPTEG:CPH nanoparticle cluster to the target is closer than that of the 50:50 CPH:SA nanoparticle cluster, suggesting that the amphiphilic 50:50 CPTEG:CPH nanoparticles behave more similarly to bacteria or LPS.

In addition, we developed predictive models via partial least squares to connect experimental measurements with molecular descriptors by predicting the PCA values of Figs. 5b and 5c as a function of molecular descriptors. The combined results of the models are shown in Fig. 5d, where the horizontal axis represents DC activation and the vertical axis represents intracellular persistence. In both cases, the increasing positive value of a molecular descriptor indicates increasing pathogen-like behavior. The specific descriptors

responsible for being pathogen-like in terms of DC activation and intracellular persistence identified by our informatics methods are: i) percentage of hydroxyl end groups, ii) hydrophobicity, iii) alkyl ethers, iv) aliphatic carbons, and v) backbone oxygen moieties.

The concept of 'similarity' defined in terms of molecular descriptors and physicochemical properties is a valuable tool to screen appropriate adjuvant candidates, enhancing our understanding of the key molecular attributes responsible for optimal adjuvant activity as well as pathogen-like behavior. For example, we identified hydroxyl end groups as an important molecular feature of the 50:50 CPTEG:CPH nanoparticles. When this polymer degrades, it exposes numerous hydroxyl end groups. Identification of hydroxyl end groups as a pathogen-like characteristic is consistent with the structural components of LPS[26] and may explain the observed similarities in DC activation profiles (Fig. 4). Indeed, recent studies by Hubbell and co-workers have shown that hydroxyl end groups on nanoparticles significantly influenced complement activation and subsequent DC trafficking to lymph nodes[27]. It is striking that descriptors such as hydroxyl end groups, alkyl ethers, and backbone oxygen moieties are commonly observed molecular constituents on pathogens and that the same parameters were identified by the (blinded) informatics analysis when complementary but dissimilar experimental data (from microscopy and flow cytometry) were compared.

Finally, we demonstrated the success of utilizing a pathogen-mimicking nanoparticle vaccine to induce long-term protection against pneumonic plague. Our previous studies have shown that encapsulation of F1-V antigen into amphiphilic polyanhydride particles preserved the antigenicity of F1-V upon release[28]. In this work, we designed and tested three vaccine formulations based on 50 μg of soluble F1-V (S_{50}), S_{50} adjuvanted with 500 μg of blank 50:50 CPTEG:CPH nanoparticles (S_{50} + E_0), and 40 μg of soluble F1-V and 10 μg of encapsulated F1-V in 500 μg of 50:50 CPTEG:CPH

nanoparticles ($S_{40} + E_{10}$). C57BL/6 mice were intranasally vacci-
nated with these formulations and subsequently challenged at 280
days post-vaccination with 1200 CFU of *Y. pestis* CO92. In these
experiments, none of the mice vaccinated with S_{50} or $S_{50} + E_0$ sur-
vived the challenge, whereas all the mice treated with the $S_{40} + E_{10}$
formulation survived (Fig. 6a). Protection from the lethal challenge
was strongly correlated with the F1-V-specific antibody titer and
antibody avidity. Mice vaccinated with either $S_{50} + E_0$ or $S_{40} + E_{10}$
generated significantly higher F1-V-specific antibody titers than ani-
mals vaccinated with S_{50} (Fig. 6b). However, by 6 weeks post-vac-
cination, anti-F1-V IgG titers began to wane in mice vaccinated with
$S_{50} + E_0$. In contrast, the F1-V-specific IgG titer in $S_{40} + E_{10}$ vacci-
nated mice was sustained for 275 days. In addition to antibody titer,
we evaluated avidity as a measure of the quality of the antigen-
specific antibody. As shown in Fig. 6c, mice vaccinated with either

S_{50} or $S_{50} + E_0$ formulations developed a low avidity F1-V-specific
IgG response. In contrast, mice vaccinated with $S_{40} + E_{10}$ generated a
higher avidity anti-F1-V specific IgG antibody by 3 weeks post-
vaccination that was sustained for 275 days. Together, the data in
Fig. 6 demonstrate that the pathogen-mimicking nanoparticle vac-
cine successfully protected animals against a lethal *Y. pestis* challenge
280 days after a single intranasal administration.

The ability to induce high titer antibody responses to F1-V fol-
lowing intranasal vaccination has been shown to be important for the
protection of mice against pneumonic *Y. pestis* infections[29-31]. Each
of these studies demonstrated the ability to induce high titer antibody
responses to F1 and/or V; however, high titer antibody responses did
not always correlate with protection. This suggests that the quality (i.e.,
avidity) of the antibody response may also be a critical factor in a
protective immune response. In this regard, the studies reported herein
have demonstrated that the use of a polyanhydride nanoparticle-
based vaccine induced long-lived, high titer, and high avidity anti-
F1-V antibody responses following a single intranasal vaccination.
Unlike the previous studies, these responses were induced without
the use of alum or TLR ligands. Similar to that induced by a natural
infection, the robustness of the immune response induced by a single
administration of the nanoparticles was remarkable in that complete
protection of mice from *Y. pestis*-induced pneumonia was observed for
at least 280 days post-vaccination.

Discussion

An ideal vaccine delivery system should consist of non-toxic materi-
als that mimic the immune enhancing capabilities of PAMPs and
activate APCs without deleterious side effects. Our results dem-
onstrate that by combining cell population-based and individual
cell-based analyses with informatics, the molecular properties
responsible for the "pathogen-mimicking" behavior of amphiphilic
nanoparticles can be identified. The ability to change size and shape
as a result of interacting with the cell, without being eliminated, was
best exhibited by the 50:50 CPTEG:CPH nanoparticles. This obser-
vation can be equated to the intracellular persistence and survival
of many microbial pathogens including *Brucella, Salmonella,* and
Mycobacterium species[32]. Moreover, the 50:50 CPTEG:CPH nano-
particles possessed the ability to enhance DC activation similar to
LPS without inducing a toxic cytokine storm. The informatics ana-
lysis confirmed the similarity between 50:50 CPTEG:CPH nano-
particles and bacteria/LPS and identified the molecular descriptors
responsible for their similarity in terms of intracellular persistence
and DC activation. Vaccination of mice with 50:50 CPTEG:CPH
nanoparticles administered as a single intranasal dose induced
high-titer and high-avidity antibody responses and 100% protection
against a live *Y. pestis* challenge for at least 280 days post-vaccination.

Our transdisciplinary approach to adjuvant design provides a tool-
box that can be used to rationally identify and design "pathogen-
mimicking" materials for use in combination vaccines that will
induce the appropriate immune modulation to protect against a wide
range of pathogens. We hypothesize that the insights gained by our
approach will elucidate important principles of rational design of
adjuvants. We foresee that the immunological and public health
challenges associated with the control of emerging and re-emerging
infectious diseases may not be met by the use of off-the-shelf adju-
vants and delivery systems that must be supplemented with TLR
ligands or excipients and administered multiple times to obtain
protection[33]. Instead, these challenges will likely require the develop-
ment of novel vaccine delivery platforms that appropriately modu-
late the immune response and improve patient compliance by
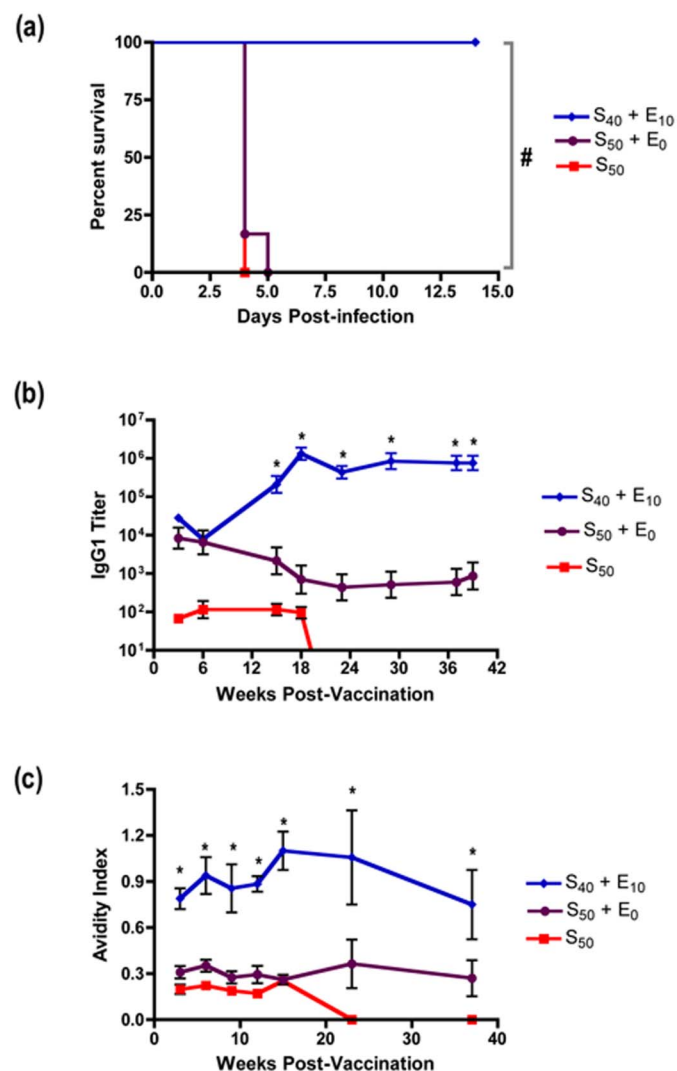requiring only a single administration.

**Figure 6 | Single administration of 50:50 CPTEG:CPH nanoparticle
vaccine provided complete protection against lethal *Y. pestis* challenge
and induced a long-lived, high-titer, high-avidity antibody response.**
(a) C57BL/6 mice were challenged intranasally with 1200 CFU (LD100) *Y.
pestis* CO92 at 280 days post intranasal vaccination (n = 5−6 per group).
(b) Kinetics of IgG antibody titer throughout 275 days post-vaccination
(n = 6 per group). (c) Kinetics of IgG antibody avidity throughout 275 days
post vaccination (n = 6 per group). Titer and avidity data are presented as
mean ± SEM. For (a), # represents a statistically significant difference from
all other treatments at $p \leq 0.0016$ and for (b) and (c) * represents a
statistically significant difference from all other treatments at $p \leq 0.05$.

Methods

(St. Louis, MO); 4-*p*-fluorobenzonitrile (98%) purchased from Apollo Scientific (Stockport, Cheshire, England); and sodium hydroxide, sulfuric acid, acetonitrile, dimethyl formamide, toluene and potassium carbonate purchased from Fisher Scientific (Fairlawn, NJ). Acetic anhydride, chloroform, petroleum ether, ethyl ether, methylene chloride and hexanes were purchased from Fisher Scientific. DC culture medium included RPMI 1640, HEPES buffer, L-glutamate, penicillin-streptomycin, gentamycin acquired from Mediatech (Herndon, VA); heat inactivated fetal calf serum acquired from Atlanta Biologicals (Atlanta, GA); and GM-CSF acquired from PeproTech (Rocky Hill, NJ). Materials used in flow cytometry included fixative buffer (BD Bioscience); mouse serum; anti-mouse CD16/32 FcγR purchased from eBioscience (San Diego, CA); β-mercaptoethanol and unlabeled rat immunoglobulin purchased from Sigma Aldrich; *E. coli* lipopolysaccharide (LPS) was acquired from Sigma Aldrich. FluoSpheres® (200 nm and 2 μm) were purchased from Invitrogen (Carlsbad, CA). *Y. pestis*, strain CO92 (NR-641) and the *Y. pestis* F1-V fusion protein, recombinant from *E. coli* (NR-4525), were obtained from the Biodefense and Emerging Infections Repository (Manassas, VA).

Polymer Synthesis, Nanoparticle Fabrication, and Characterization. Sebacic acid was purchased from Sigma Aldrich. Synthesis of CPTEG and CPH diacids, SA and CPH pre-polymers, and CPH:SA and CPTEG:CPH copolymers was performed as previously described[34,35]. The polymers were characterized using ^{1}H nuclear magnetic resonance spectroscopy, gel permeation chromatography, and differential scanning calorimetry. All properties evaluated of the synthesized polymers were within accepted ranges[34,35].

Both FITC-dextran loaded and blank nanoparticles were fabricated using the protocol reported in Ulery et al.[13]. The endotoxin levels of these particles were tested using a *Limulus* Amebocyte Lysate (LAL) QCL-1000 test kit (Cambrex, Walkersville, MD) as described previously[12]. The results indicated that the particles exhibited an endotoxin content of less than 0.1 EU/mL, which is five times lower than the maximum level permitted by the United States FDA for new drugs tested by the LAL test[36]. Nanoparticle morphology and size was investigated using scanning electron microscopy (JEOL 840A, JEOL Ltd., Tokyo, Japan) and appeared to be spherical in shape. The size of the 50:50 CPTEG:CPH nanoparticles was 206 ± 47 nm and that of the 50:50 CPH:SA nanoparticles was 415 ± 76 nm (data presented as mean ± standard deviation from three independent batches of nanoparticles). No differences in size or morphology were found for blank or 1% FITC-dextran-loaded nanoparticles across all chemistries.

Culture, Stimulation, and Analysis of C57BL/6 Dendritic Cells. All experiments involving animals were carried out in accordance with procedures approved by the Iowa State University Institutional Animal Care and Use Committee. The dendritic cells (DCs) were prepared from bone marrow cells isolated from the femurs, tibias, humeri and ilia of C57BL/6 mice (obtained from Harlan Sprague Dawley). DCs were cultured, stimulated and assessed for cell surface marker expression and cytokine secretion as described previously with the same materials[11]. Nanoparticle stimulation doses of 125 μg/mL and LPS stimulation doses of 200 ng/mL were utilized.

Intracellular Localization. Intracellular localization of nanoparticles was compared between PS beads at a 1:1000 dilution and 250 μg/mL of 1% FITC-dextran loaded nanoparticles composed of either 50:50 CPH:SA or 50:50 CPTEG:CPH. DCs were infected with green fluorescent protein (GFP)-expressing *E. coli* HB101 or *Y. pestis* Δpgm at multiplicity of infection (MOI) of 100 and 10, respectively. Following nine days of culture, DCs were pulsed with particles for 30 min (2 h sample) or 6 h (48 h sample). *E. coli* and *Y. pestis* were incubated for 30 min and 48 h with DCs. Cells were subjected to immunofluorescence microscopy to observe time-dependent intracellular trafficking of individual nanoparticles within DCs, similarly to previous work[13]. Polymerized actin was labeled with Alexa 568 conjugated phalloidin mushroom toxin (Molecular Probes-Invitrogen) and lysosomes were stained with ID-4B anti-LAMP-1 (lysosomal-associated membrane protein 1). Epifluorescence and immunofluorescence microscopy were performed using an inverted Olympus Fluoview™ 1000 laser scanning confocal microscopy. Intracellular trafficking analysis and final images were prepared using ImageJ v1.36b (NIH, Bethesda, MD) loaded with particle counting algorithms.

Vaccinations and Challenge of Mice. *Y. pestis* CO92 was grown overnight at 37°C in heart-infusion broth supplemented with 0.2% D-galactose. Eight-week-old female C57BL/6 mice were obtained from the Jackson Laboratory (Bar Harbor, ME) and maintained under SPF conditions. The Institutional Committees on Animal Care and Use at either Iowa State University or Albany Medical College approved all procedures involving animals. Mice were vaccinated and challenged and the methods to measure antibody titer and avidity were performed as described previously[5].

Data and Statistical Analysis. JMP software (SAS Institute, Cary, NC) was used to make comparisons between treatments and the negative (NS) control and the positive (LPS) control using the student T-test.

Informatics Analysis. The similarity matrix shown in Fig. 5a was constructed with the correlation (R) metric defined by the following equation:

$$R(x,y) = \frac{\text{cov}(x,y)}{\sigma_x \sigma_y} = \frac{\sum_{i=1}^{n}(x_i - x_{mean})(y_i - y_{mean})}{\sqrt{\sum_{i=1}^{n}(x_i - x_{mean})^2}\sqrt{\sum_{i=1}^{n}(y_i - y_{mean})^2}}$$

Here, x and y refer to a block of chemistries (LPS, 20:80 CPTEG:CPH, 50:50 CPTEG:CPH, 20:80 CPH:SA, 50:50 CPH:SA, poly(CPTEG), poly(CPH), and poly(SA)), cov(x,y) is the covariance between x chemistry and y chemistry, and σ is the standard deviation. Note that only molecular descriptors 1–25 and 28 from Table 1 were used to generate this similarity matrix.

The PCA analysis for nanoparticle persistence (Fig. 5b) used count, total area, and average size from epifluorescence microscopy data, while that for DC activation (Fig. 5c) used MHC I, MHC II, CD40, CD86, IL-6, IL-12p40, and TNF-α data. PLS regression connected the descriptor data set with the results of the PC analyses. By projecting the data onto a high-dimensional hyperplane defined by PCA analysis of training data, the impact of the descriptors on the property were identified, while taking co-linearity into account[37].

1. Zepp, F. Principles of vaccine design-lessons from nature. *Vaccine* **28**, C14–C24 (2010).
2. Moser, M. & Leo, O. Key concepts in immunology. *Vaccine* **28**, C2–C13 (2010).
3. Kipper, M. J., Wilson, J. H., Wannemuehler, M. J., & Narasimhan, B. Single dose vaccine based on biodegradable polyanhydride microspheres can modulate immune response mechanism. *J Biomed Mater Res A* **76A**, 798–810 (2006).
4. Pawar, D. *et al*. Evaluation of mucoadhesive PLGA microparticles for nasal immunization. *Aaps J* **12**, 130–137 (2010).
5. Ulery, B. D. *et al*. Design of a protective single-dose intranasal nanoparticle-based vaccine platform for respiratory infectious diseases. *PLoS ONE* **6**, e17642 (2011).
6. Coeshott, C. M. *et al*. Pluronic® F127-based systemic vaccine delivery systems. *Vaccine* **22**, 2396–2405 (2004).
7. Andrianov, A. K., Townsend, H. & Mutwiri, G. Poly[di(carboxylatophenoxy)phosphazene] is a potent adjuvant for intradermal immunization. *Proc Natl Acad Sci U S A* **106**, 18936–18941 (2009).
8. Wilson-Welder, J. H. *et al*. Vaccine adjuvants: Current challenges and future approaches. *J Pharm Sci* **98**, 1278–316 (2009).
9. Determan, A. S. *et al*. Encapsulation, stabilization, and release of BSA-FITC from polyanhydride microspheres. *J Control Release* **100**, 97–109 (2004).
10. Torres, M. P. *et al*. Amphiphilic polyanhydrides for protein stabilization and release. *Biomaterials* **28**, 108–16 (2007).
11. Petersen, L. K. *et al*. The simultaneous effect of polymer chemistry and device geometry on the in vitro activation of murine dendritic cells. *Biomaterials* **30**, 5131–5142 (2009).
12. Torres, M. P. *et al*. Polyanhydride microparticles enhance dendritic cell antigen presentation and activation. *Acta Biomater* **7**, 2857–2864 (2011).
13. Ulery, B. D. *et al*. Polymer chemistry influences monocytic uptake of polyanhydride nanospheres. *Pharm Res* **26**, 683–690 (2009).
14. Janeway, C. A., Travers, P., Shlomichik, M. J. & Walport, M. *Immunobiology* (Garland Science, New York, 2005).
15. InvivoGen, Agonistic and antagonistic effects of LPS on TLR4. www.invivogen.com (January 11 2011).
16. Gatti, E. & Pierre, P. Understanding the cell biology of antigen presentation: the dendritic cell contribution. *Curr Opin Cell Biol* **15**, 468–473 (2003).
17. Gallucci, S., Lolkema, M. & Matzinger, P. Natural adjuvants: Endogenous activators of dendritic cells. *Nat Med* **5**, 1249–1255 (1999).
18. Hu, Y. *et al*. Cytosolic delivery of membrane-impermeable molecules in dendritic cells using pH-responsive core-shell nanoparticles. *Nano Lett* **7**, 3056–3064 (2007).
19. Watts, C. Antigen processing in the endocytic compartment. *Curr Opin Immunol* **13**, 26-31 (2001).
20. Gold, J. A. *et al*. CD40 contributes to lethality in acute sepsis: *in vivo* role for CD40 in innate immunity. *Infect Immun* **71**, 3521–8 (2003).
21. Bicerano, J. *Predictions of Polymer Properties*. (Marcel Dekker, New York; 1996).
22. Rodriguez-Torres, A. *et al*. Differential scanning calorimetry investigations on LPS and free lipids A of the bacterial cell wall. *Res Microbiol* **144**, 729–40 (1993).
23. Ramos-Sanchez, M. C. *et al*. Thermolytical techniques to characterize fungal polysaccharides and bacterial lipopolysaccharides. *Biotechnol Prog* **7**, 526–33 (1991).
24. Pearson, K. Mathematical contributions to the theory of evolutions. III. Regression, heredity, and panmixia. *Philos Trans R Soc London A* **187**, 253–318 (1896).
25. Broderick, S. R., Nowers, J. R., Narasimhan, B. & Rajan, K. Tracking chemical processing pathways in combinatorial polymer libraries via data mining. *J Comb Chem* **12**, 270–277 (2010).
26. Erridge, C., Bennett-Guerrero, E. & Poxton, I. R. Structure and function of lipopolysaccharides. *Microbes Infect* **4**, 837–51 (2002).
27. Reddy, S. T. *et al*. Exploiting lymphatic transport and complement activation in nanoparticle vaccines. *Nat Biotechnol* **25**, 1159–64 (2007).
28. Carrillo-Conde, B. *et al*. Encapsulation into amphiphilic polyanhydride microparticles stabilizes *Yersinia pestis* antigens. *Acta Biomater* **6**, 3110–9 (2010).
29. Airhart, C. L., *et al*. Lipid A mimetics are potent adjuvants for an intranasal pneumonic plague vaccine. *Vaccine* **26**, 5554–5561 (2008).
30. Amemiya, K. *et al*. CpG oligodeoxynucleotides augment the murine immune response to the *Yersinia pestis* F1-V vaccine in bubonic and pneumonic models of plague. *Vaccine* **27**, 2220–2229 (2009).

31. Huang, J. *et al*. Protective immunity in mice achieved with dry powder formulation and alternative delivery of plague F1-V vaccine. *Clin Vaccine Immunol* **16**, 719–25 (2009).
32. Diacovich, L. & Gorvel, J. P. Bacterial manipulation of innate immunity to promote infection. *Nat Rev Microbiol* **8**, 117–128 (2010).
33. Kasturi, S. P. *et al*. Programming the magnitude and persistence of antibody responses with innate immunity. *Nature* **470**, 543–7 (2011).
34. Kipper, M. J., Shen, E., Determan, A. & Narasimhan, B. Design of an injectable system based on bioerodible polyanhydride microspheres for sustained drug delivery. *Biomaterials* **23**, 4405–12 (2002).
35. Torres, M. P., Vogel, B. M., Narasimhan, B. & Mallapragada, S. K. Synthesis and characterization of novel polyanhydrides with tailored erosion mechanisms. *J Biomed Mater Res A* **76**, 102–10 (2006).
36. Guideline on validation of the *Limulus* amebocyte test as an end-product endotoxin test for human and animal parenteral drugs, biological products, and medical devices. *Center for Drug Evaluation and Research*. 1–10 (1987).
37. Rosipal, R. & Kramer, N. *Subspace, Latent Structure and Feature Selection Techniques* (Springer, Berlin/Heidelberg, 2006).

Acknowledgements

Author contributions

Additional information